Supporting Information

Hydrogen spillover effect - Harnessing Hydrogen Evolution Reaction from Diverse Carbon-based Supports with Tungsten Oxide Catalyst

R Rajalakshmi, G Srividhya, C Viswanathan, N Ponpandian*

Department of Nanoscience and Technology, Bharathiar University, Coimbatore, India.

Table of contents:

Supplementary figures

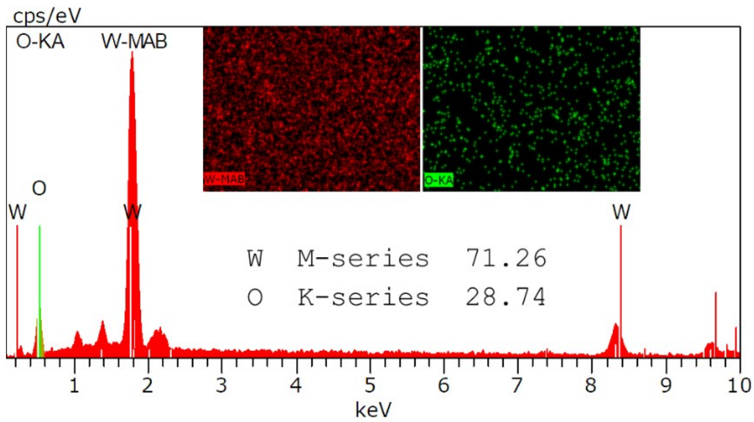

Figure S1. EDAX and elemental mapping of WO_3 nanorods.

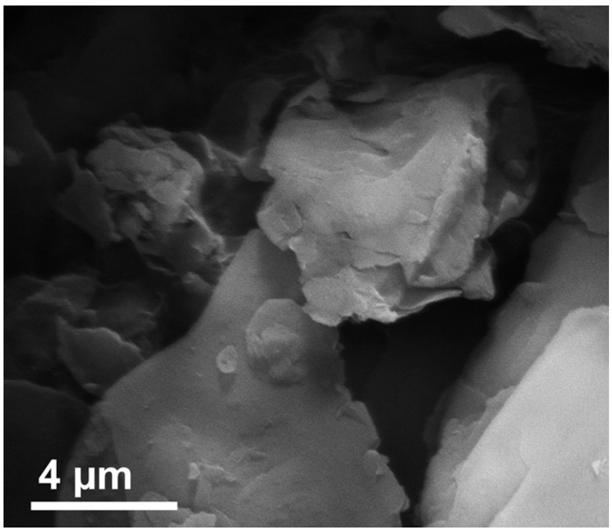

Figure S2. FESEM image of pristine graphene oxide (GO)

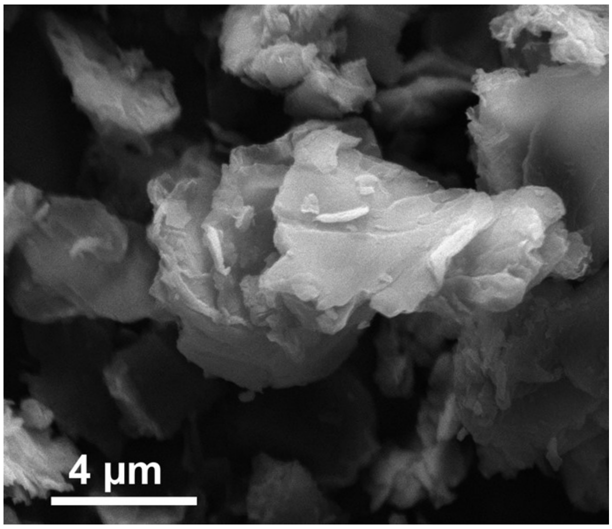

Figure S3. FESEM image of pristine reduced graphene oxide (rGO)

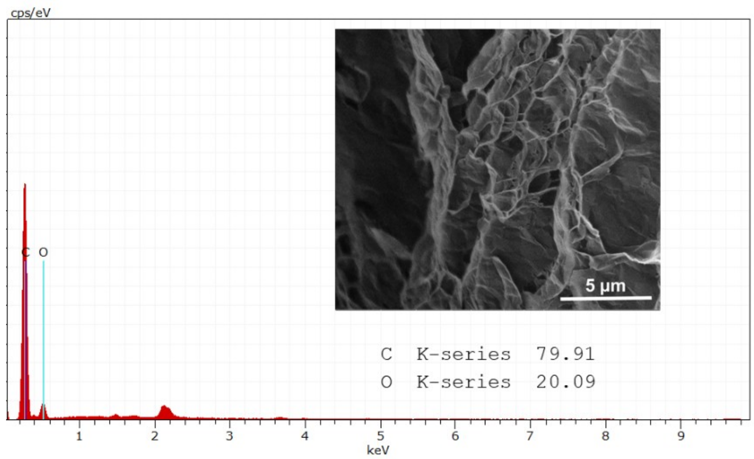

Figure S4. EDAX representing the carbon and oxygen content of reduced graphene sheets (GR). Inset represents the FESEM image of multilayered reduced graphene sheets.

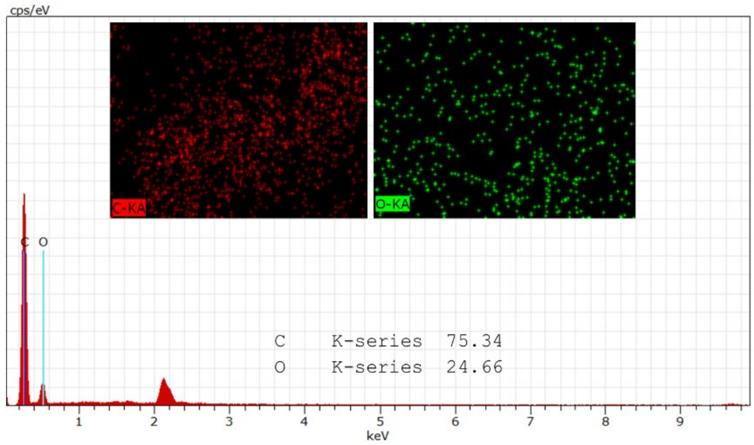

Figure S5. EDAX and elemental mapping of reduced graphene oxide (rGO).

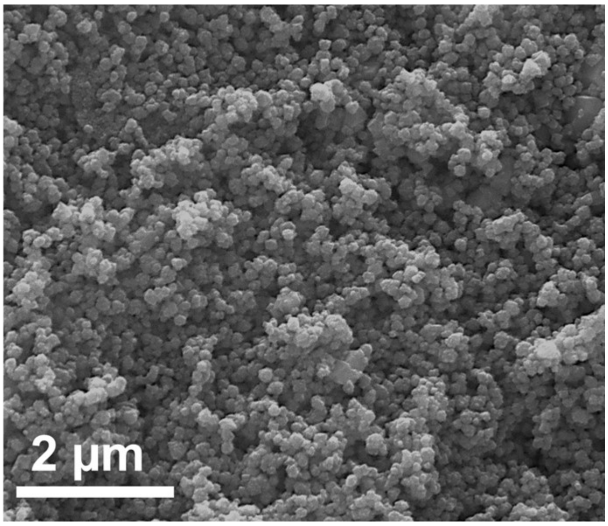

Figure S6. FESEM image of as purchased carbon black sub-micro particles (CB)

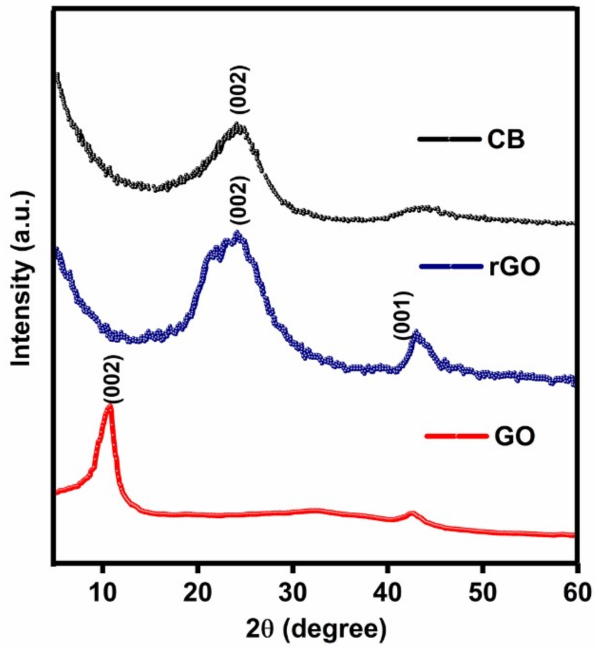

Figure S7. X-Ray diffraction patterns of GO, rGO and CB.

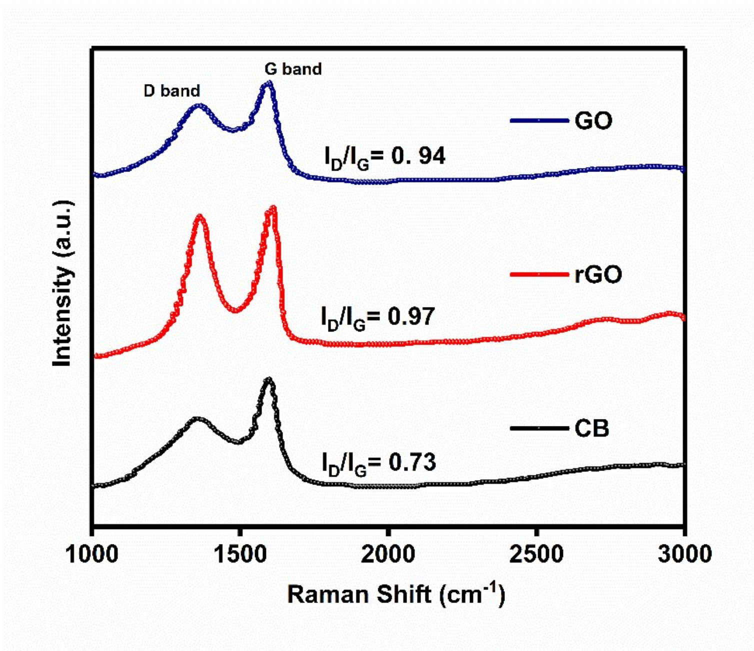

Figure S8. Raman spectra of GO, rGO and CB.

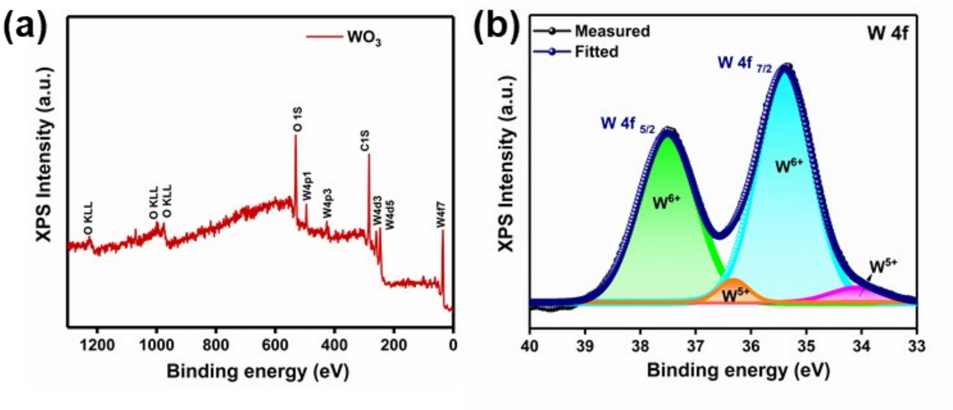

Figure S9. (a) XPS spectra of pristine WO_3 and (b) the deconvoluted XPS spectra of W 4f.

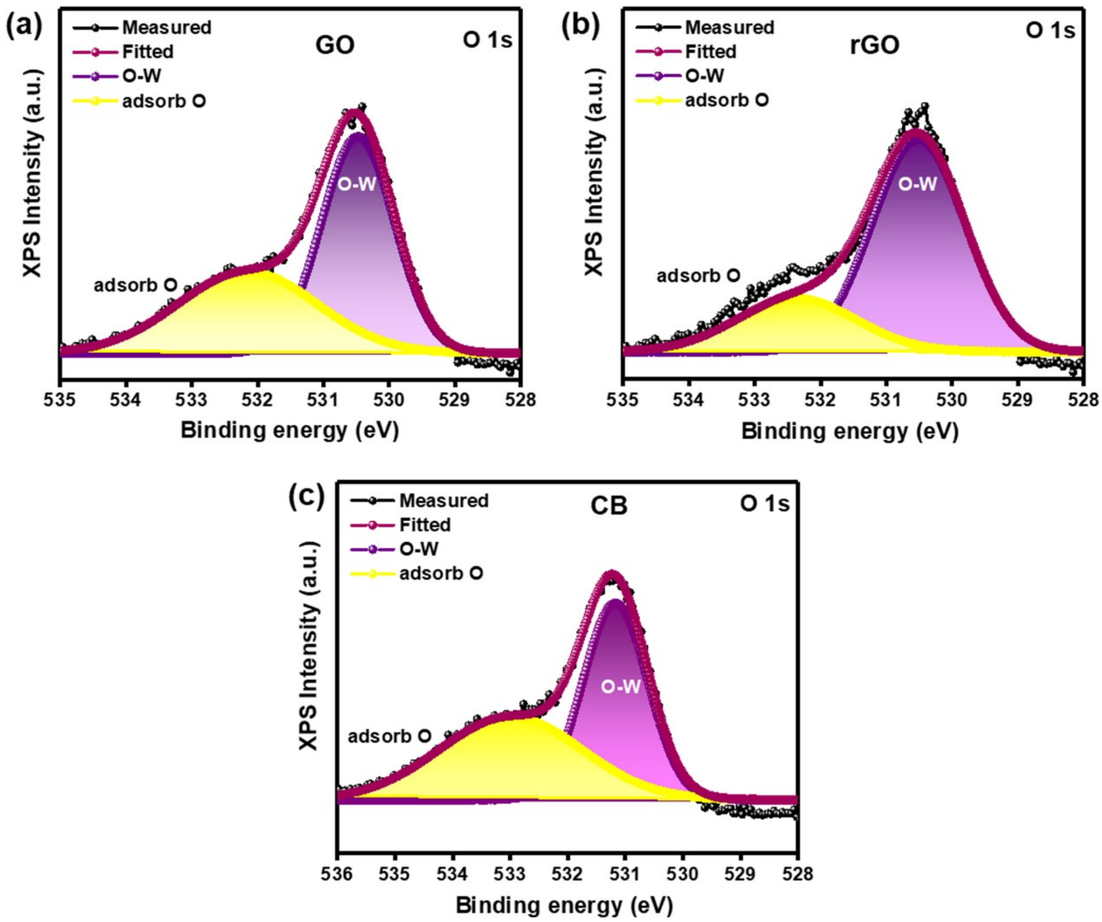

Figure S10. Deconvoluted XPS spectra of O1s of (a) WO_3/GO, (b) WO_3/rGO, and (c) WO_3/CB,

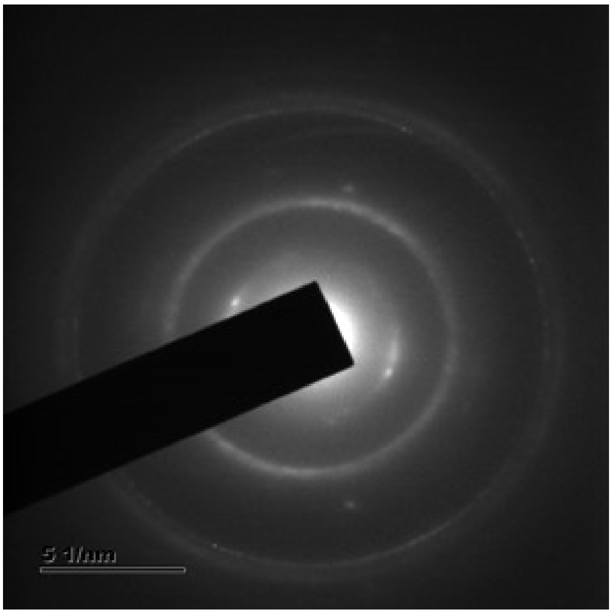

Figure S11. SAED pattern of graphene sheets.

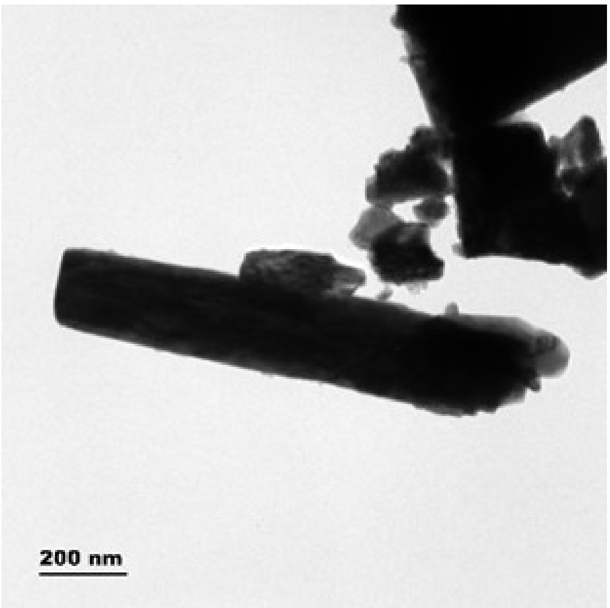

Figure S12. TEM image of WO_3 nanorods.

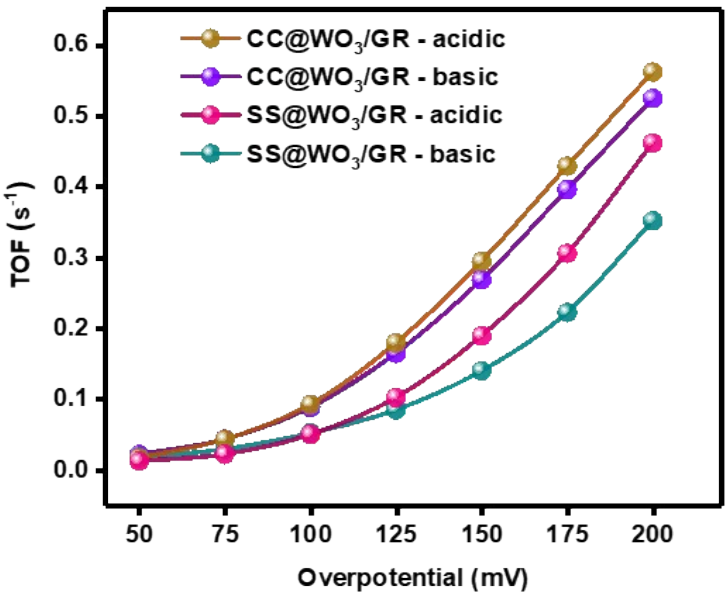

Figure S13 - The turnover frequency (TOF) of CC@WO_3/GR and SS@WO_3/GR in both the acidic and basic electrolytes at different overpotential values related to the H_2 gas production.

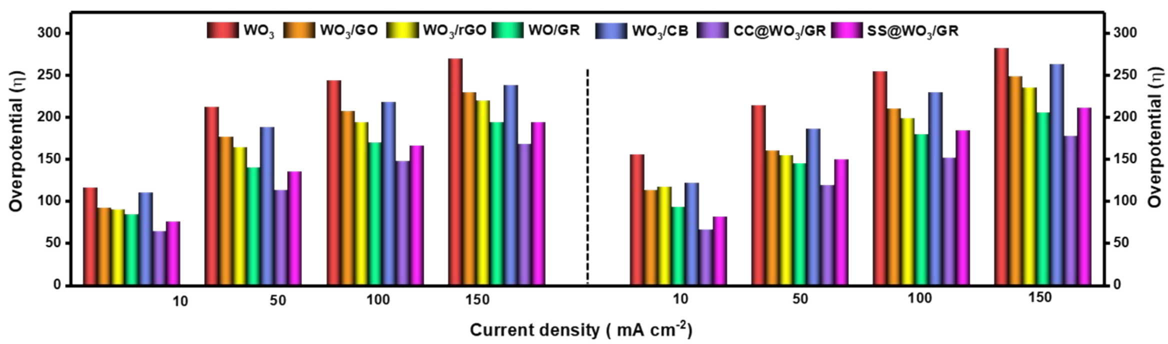

Figure S14. Comparison of overpotential values of all the electrocatalysts of WO_3 at different intervals of current density.

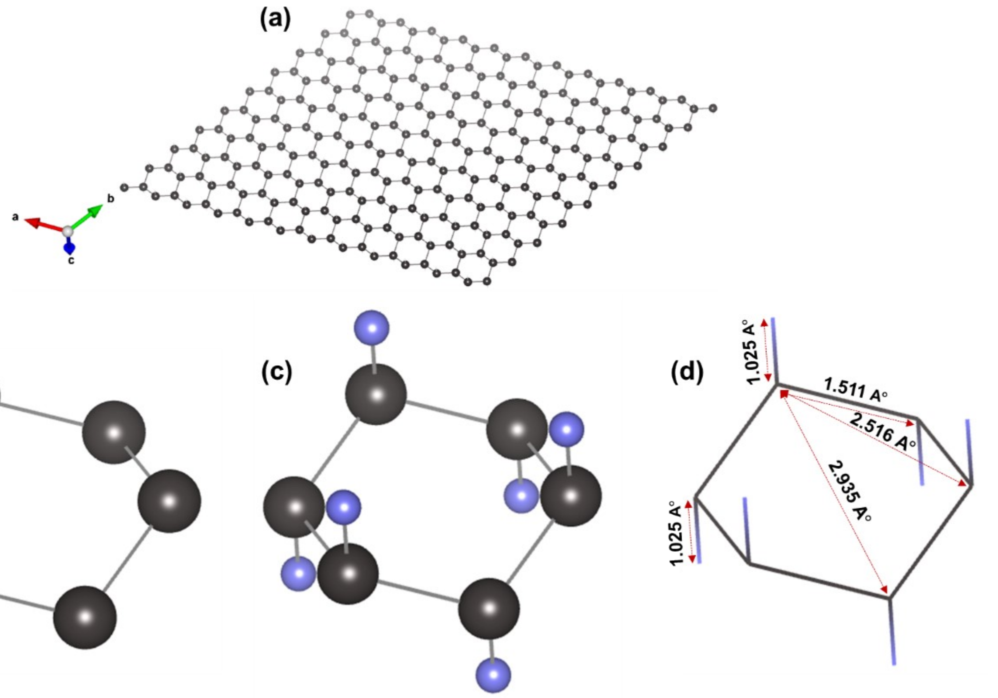

Figure S15. (a) Graphene sheet, (b) single graphene in Ball and stick model, (c) graphene in ball and stick model and (d) the bond angles representing in the wireframe model.

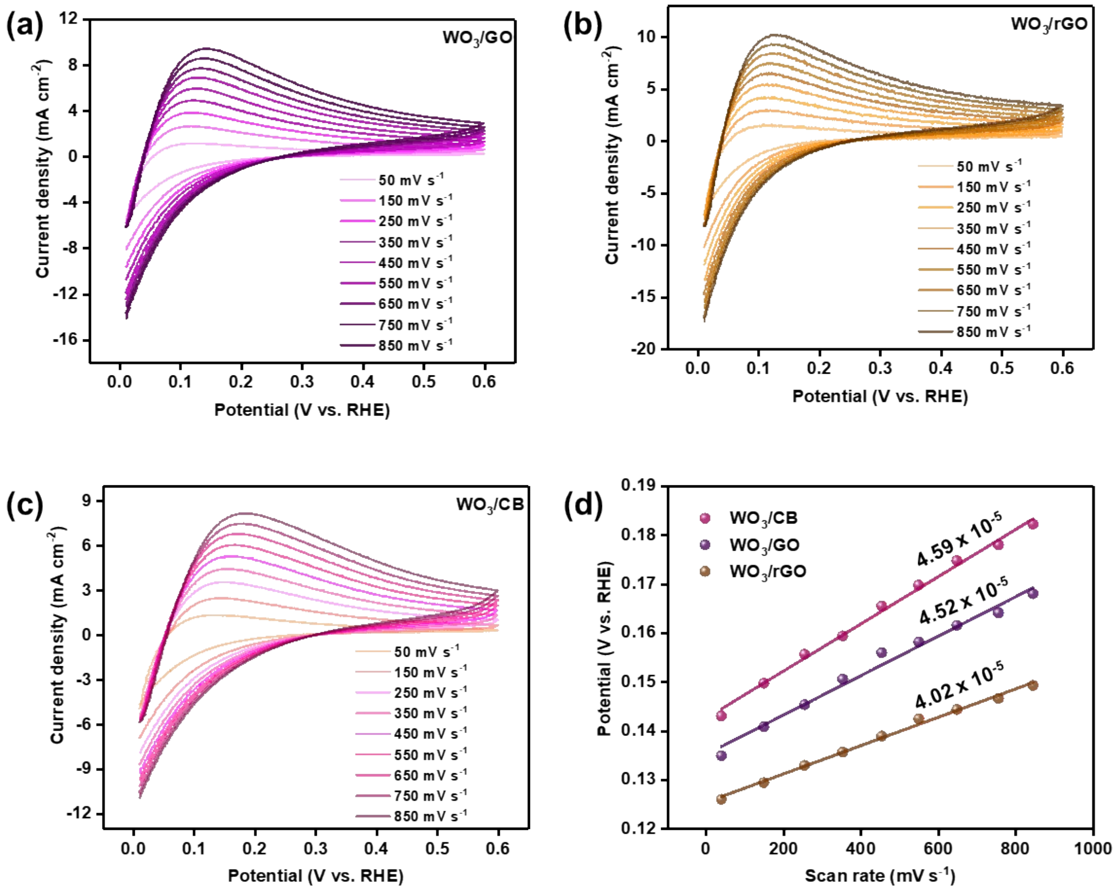

Figure S16. Cyclic voltammetry curves of (a) WO_3/GO, (b) WO_3/rGO, and (c) WO_3/CB electrocatalyst at different scan rates indicating the hydrogen desorption peaks. (d) The slope values of the desorption peak at different potential values vs the scan rate values to determine the slope values of all three carbon-based electrocatalysts.

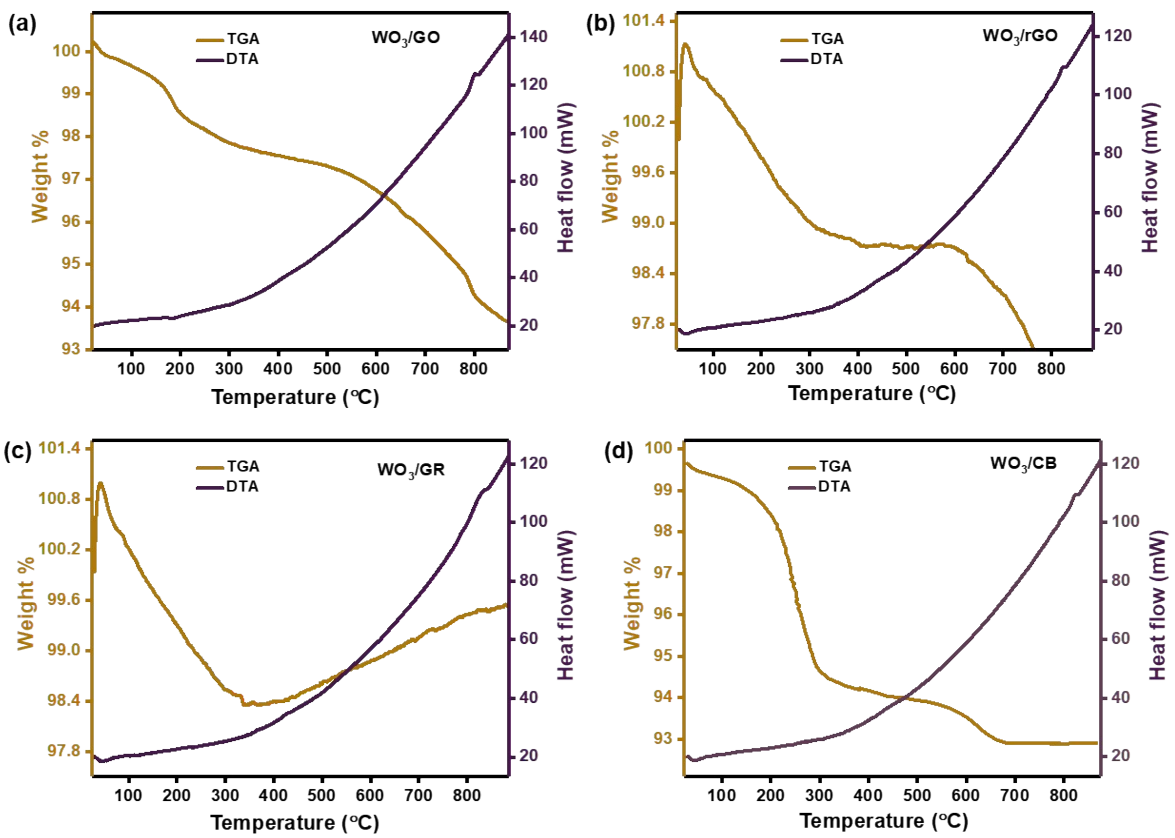

Figure S17. TGA and DTA curves of (a) WO_3/GO, (b) WO_3–rGO, (c) WO_3/GR, and (d) WO_3/CB electrocatalysts respectively.

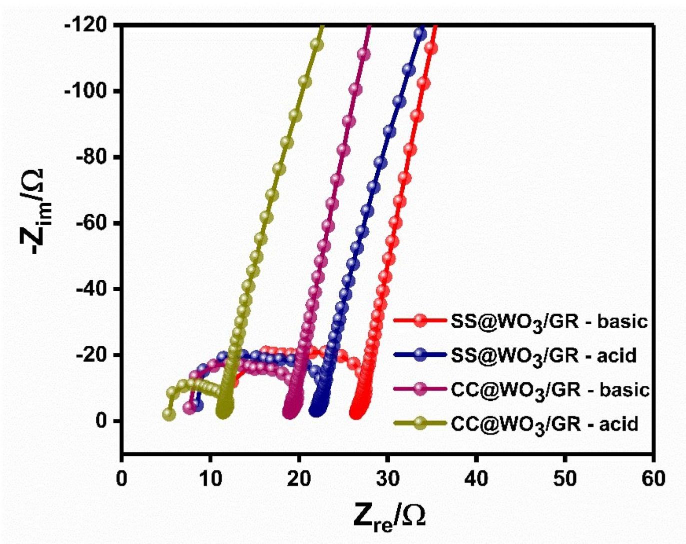

Figure S18. Enlarged area of Fig. 5a representing the solution resistance and the faradaic impedance.

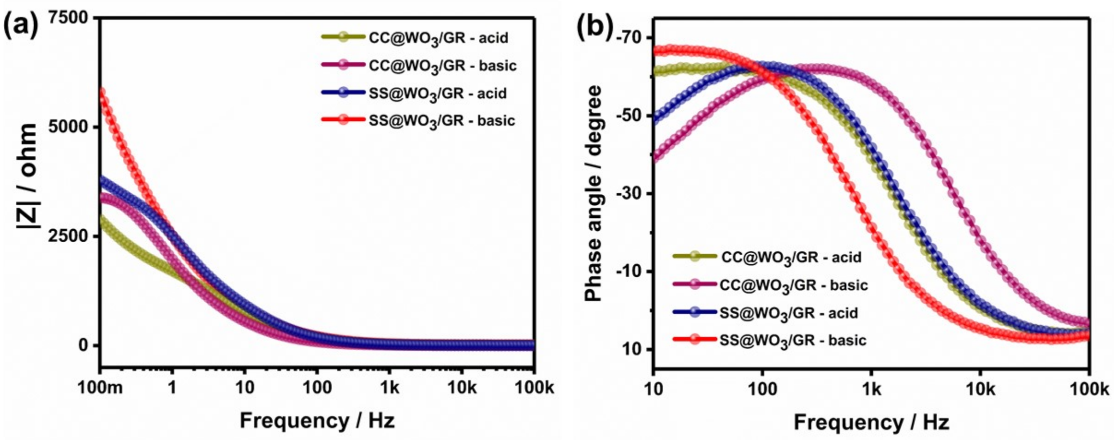

Figure S19. (a) The phase angle and (b) cut off frequency measurements of the WO_3/GR electrocatalyst deposited on CC and SS substrates in both the electrolytic mediums.

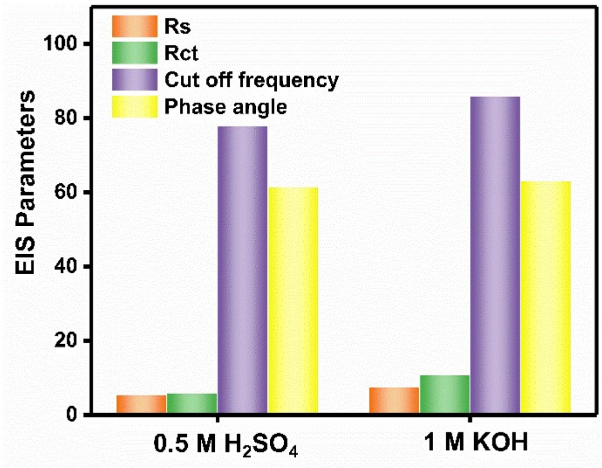

Figure S20. Comparison of the solution resistance, charge transfer resistance, cut of frequency and phase angle of CC@WO_3/GR electrocatalyst in acidic and basic electrolytes.

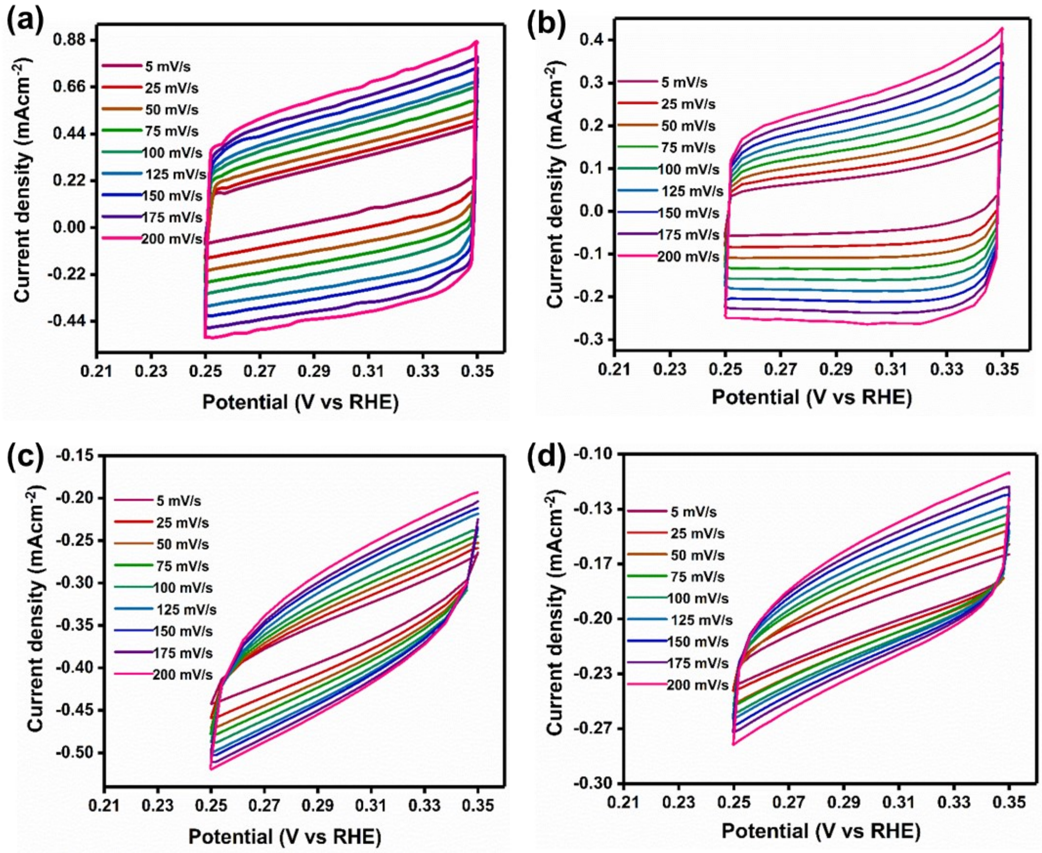

Figure S21. Cyclic voltagramms of (a) CC@WO_3/GR - 0.5 M H_2SO_4, (b) CC@WO_3/GR - 1M KOH, (c) SS@WO_3/GR - 0.5 M H_2SO_4, (d) SS@WO_3/GR - 1M KOH swept in the non-faradaic region at different intervals of san rate from 5- 200 mV/s.

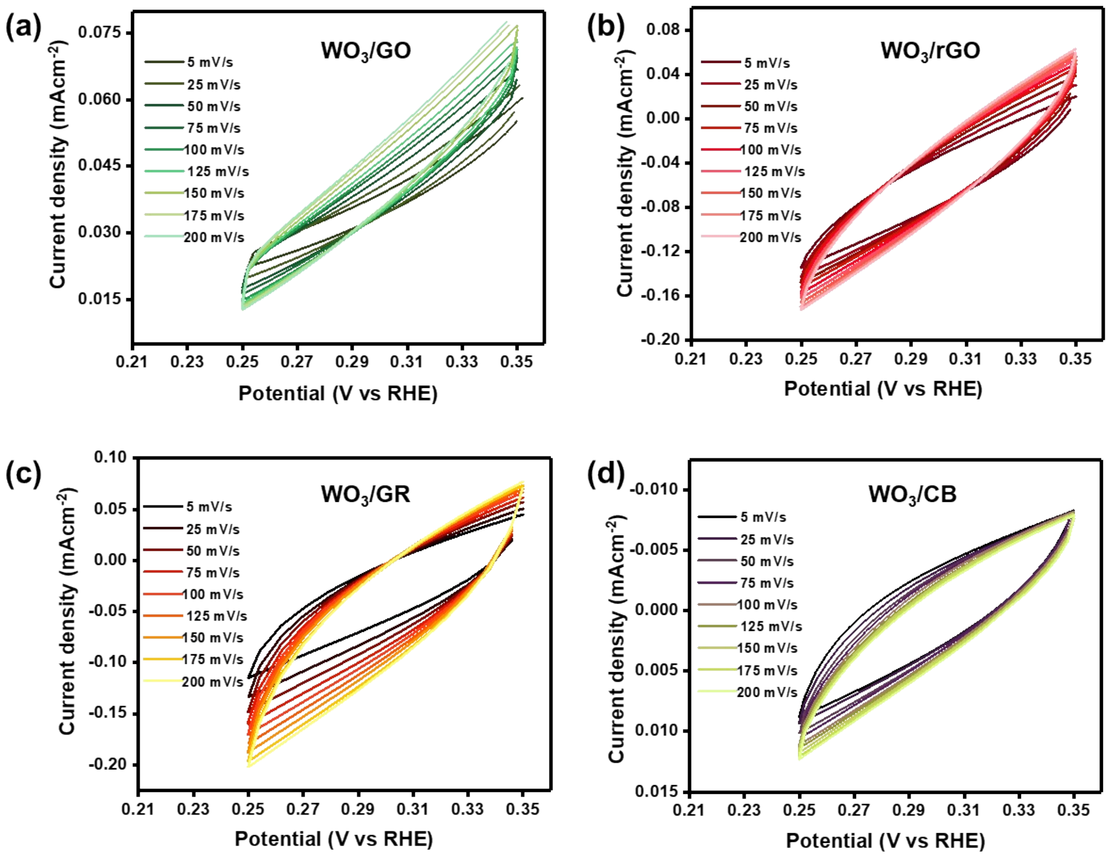

Figure S22. Cyclic voltagramms of (a) WO_3/GO, (b) WO_3/rGO, (c) WO_3/GR, and (d) WO_3/CB in 0.5 M H_2SO_4 swept in the non-faradaic region at different intervals of san rate from 5- 200 mV/s.

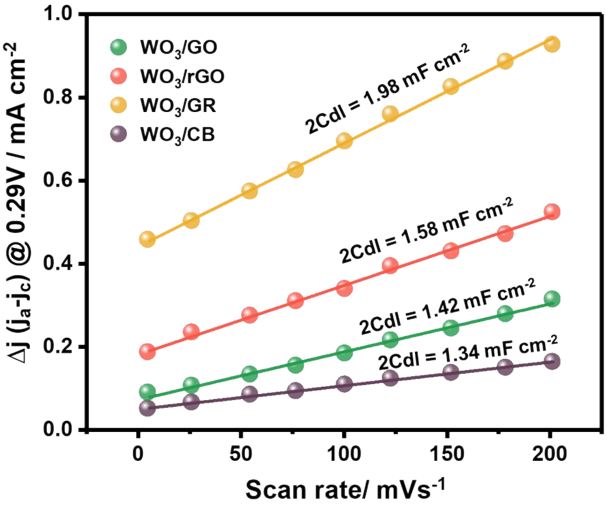

Figure S23. The capacitance obtained from the fit of double-layer charging current density versus scan rate for WO_3/GO, WO_3/rGO, WO_3/GR, and WO_3/CB electrocatalysts in acidic 0.5 M H_2SO_4 electrolyte

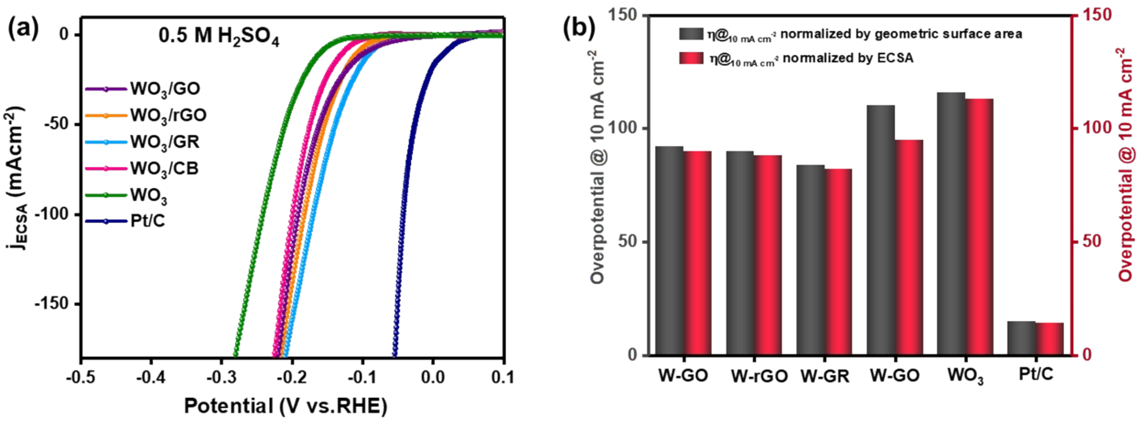

Figure S24. (a) LSV normalized curves of the electrocatalysts WO_3/GO, WO_3/rGO, WO_3/GR, and WO_3/CB with respect to electrochemical active surface area and (b) the comparison of the overpotential values at 10 mA cm^{-2} with respect to geometric surface area and the electrochemical active surface area.

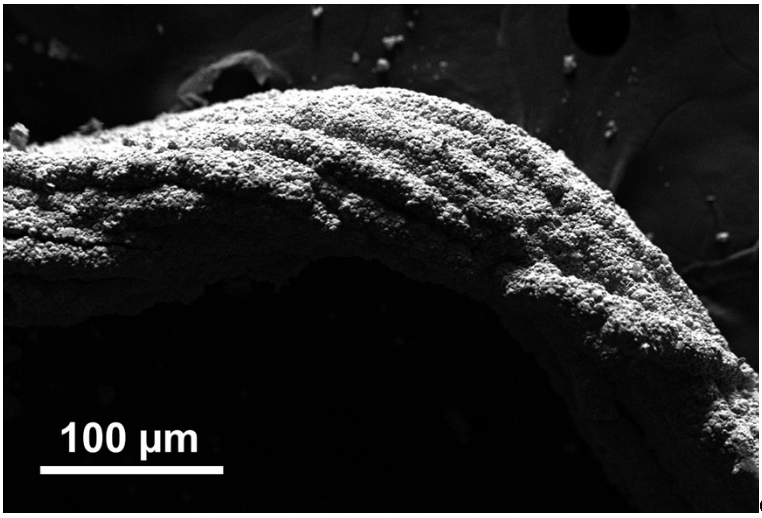

cal

Figure S25. A portion of CC@WO_3/GR electrocatalyst after the HER long term stability test.

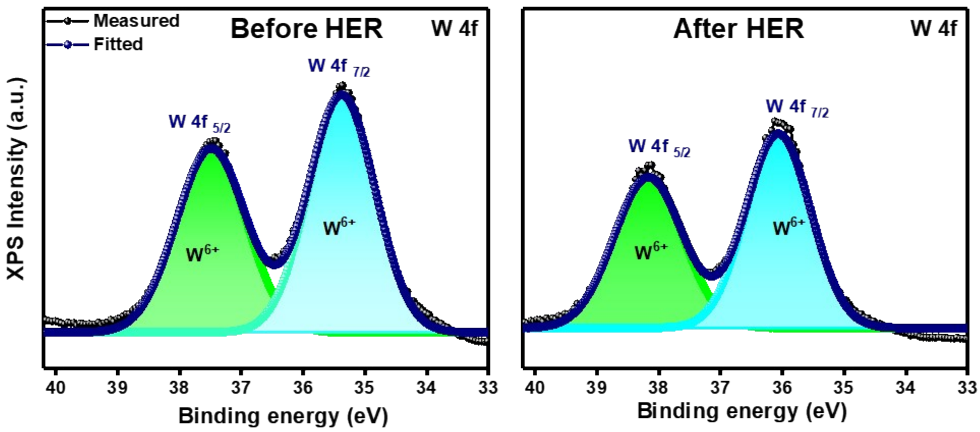

Figure S26. Deconvoluted spectra of W4f before and after the HER long term stability test.

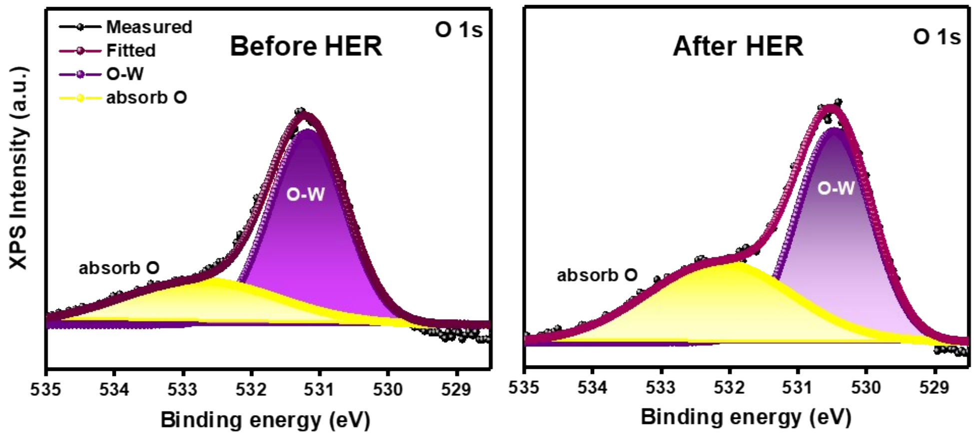

Figure S27. Deconvoluted spectra of O1s before and after the HER long term stability test.

Supplementary Table

Table S1: The overpotential at η = 10 mA cm^{-2} and Tafel slope values of all the studied electrocatalysts of WO_3 in both acidic and basic electrolytic mediums.

S. No	Electrocatalyst	Overpotential at η = 10 mA cm^{-2}		Tafel slope	
		0.5 M H_2SO_4	1 M KOH	0.5M H_2SO_4	1 M KOH
1.	WO_3	116	155	98	107
2.	WO_3/GO	92	113	74	83
3.	WO_3/rGO	90	117	70	78
4.	WO_3/GR	84	93	66	72
5.	WO_3/CB	110	122	86	89
6.	CC@WO_3/GR	64	78	54	58
7.	SS@WO_3/GR	76	83	62	69
8.	Pt/C	15	17	29	32

Table S2: Mechanism of Hydrogen evolution reaction in acidic and alkaline electrolytes

	Acid	**Alkaline**	**Tafel slope**
Overall	$^* + 2H^+ + 2e^- \rightarrow H_2$	$^* + 2H_2O + 2e^- \rightarrow H_2 + 2OH^-$	$\eta = a + b \log(-j)$
Volmer	$^* + H^+ + e^- \rightarrow H^*$	$^* + H_2O + e^- \rightarrow H^* + OH^-$	$b = 2.3RT/\alpha F$ ~120 mV/dec
Heyrovsky	$^* + H^+ + e^- + H^* \rightarrow H_2 + ^*$	$^* + H_2O + e^- + H^* \rightarrow H_2 + OH^- + ^*$	$b = 2.3RT/(1+\alpha)F$ ~40 mV/dec
Tafel	$2H^* \rightarrow H_2 + 2^*$	$2H^* \rightarrow H_2 + 2^*$	$b = 2.3RT/2F$ ~30 mV/dec
Where " * " denotes the active site on the surface of the electrocatalyst.			

Table S3: The Nernst equation and coupling processes necessary to produce the three dimensional Tungsten Pourbaix diagram at T = 298 K.

No	**Species**	**Reaction**	**Nernst equation**
1.	$WO_2(s)/W(s)$	$WO_2 + 4H^+ + 4e^- = W + 2H_2O$	E_e= -0.15 - 0.059pH
2.	$WO_3(s)/WO_2(s)$	$WO_3 + 2H^+ + 2e^- = WO_2 + H_2O$	E_e= 0.038 - 0.059pH
3.	$WO_3(s)/ HW_6O_{21}^{5-}(aq)$	$6WO_3 + 3H_2O = HW_6O_{21}^{5-} + 5H^+$	5pH = log $[HW_6O_{21}^{5-}]$ + 20.92
4.	$HW_6O_{21}^{5-}(aq)/WO_4^{2-}$ (aq)	$HW_6O_{21}^{5-} + 3H_2O = 6WO_4^{2-} + 7H^+$	7pH = 6log $[WO_4^{2-}]$ – log $[HW_6O_{21}^{5-}]$ + 67.82
5.	$WO_3(s)/ WO_4^{2-}$ (aq)	$WO_3 + H_2O = WO_4^{2-} + 2H^+$	2pH = log$[WO_4^{2-}]$ + 14.79
6.	WO_4^{2-} (aq)/ W(s)	$WO_4^{2-} + 8H^+ + 6e^- = W + 4H_2O$	E_e= 0.06 + 0.01log$[WO_4^{2-}]$ – 0.079pH
7.	WO_4^{2-} (aq)/ $WO_2(s)$	$WO_4^{2-} + 4H^+ + 2e^- = WO_2 + 2H_2O$	E_e= 0.48 + 0.03log$[WO_4^{2-}]$ – 0.118 pH
8.	$HW_6O_{21}^{5-}(aq)/ WO_2(s)$	$HW_6O_{21}^{5-} + 17H^+ + 12e^- = 6WO_2 + 9H_2O$	E_e= 0.14 + 0.005log$[HW_6O_{21}^{5-}]$ – 0.084 pH

Table S4: The stable and unstable compounds when the elements W and C react to produce the Pourbaix (E-pH) plot.

Elements studied	**Stable compounds**	Unstable compounds
W (Tungsten) – 80% C (Carbon) – 20% Concentration: 10^0 mol/kg Temperature: 298 K	WO_3 (s) + CH_4 (aq) CH_4 (aq) + $W_{18}O_{49}$(s) CH_4 (aq) + W(s) W_8O_{21}(s) + CH_4 (aq) WO_3(s) + CO_2(s) WO_4^{2-} + CO_3^{2-} CH_4 (aq) + WO_4^{2-} HCO^{3-} + WO_4^{2-} WO_4^{2-} + CO_2(s)	WO_4^{2-} + CO_2 (aq) W(s) + CH_3CH_2OH (aq) W(s) + CH_3COOH (aq) WO_3(s) + CO_2 aq) WO_3(s) + CO_3^{2-} CO_2(s) + $W_{18}O_{49}$(s) $W_{18}O_{49}$(s) + CH_3CH_2OH (aq) $W_{18}O_{49}$(s) + CH_3COOH (aq)

Table S5: References of the electrocatalysts illustrated in Figure 8d.

S.No	Electrocatalyst	Reference
1.	WO_3/C@CoO	[1]
2.	Pt/def-WO_3@CFC	[2]
3.	Pt/WO_3	[2]
4.	CC@WO_3/GR	This work
5.	SS@ WO_3/GR	This work
6.	WO_3/GR	This work
7.	Fe-WO_xP/rGO	[3]
8.	WO_3/rGO	This work
9.	WO_3/GO	This work
10.	V-WO_3	[4]
11.	WSe_2/WO_3-y	[5]
12.	WO_3/CB	This work
13.	WO_3/TiO_2	[6]
14.	WO_{3-x}-CNFs	[7]
15.	CC@WO_3 – Sm 4%	[8]
16.	WS_2/WC-WO_3	[9]
17.	Mn-WO_3	[4]
18.	WO_3/MoS_2-MoOx	[10]
19.	$CoSe_2$/WSe_2/WO_3@CC	[11]
20.	WO_3.2H_2O/WS_2	[12]
21.	WO_3-Sm 4%	[8]
22.	WS_2-WO_3-CNF	[13]
23.	Pd@WO_3	[14]
24.	$CoSe_2$-WO_3	[11]
25.	MoS_2@WO_3	[10]
26.	WO_3/NPRGO	[15]
27.	Meso-$WO_{2.83}$	[16]
28.	WS_2-WO_3	[17]
29.	Ta-WO_3	[18]
30.	Zeolite/WO_3	[19]

Supplementary Calculation

The turnover frequency is calculated using the relation

$$TOF = j / (m \times F \times n)\ (s^{-1})$$

Here, j is the current density at a particular overpotential value (η in mV), m is the number of moles present in the catalyst, F is the Faraday constant (96,485.4 C mol^{-1}), and n is the number of electrons transferred to generate one molecule of hydrogen gas which is 2 [20].

To calculate the number of moles present in the active electrocatalyst - WO_3/GR, the individual number of moles of WO_3 and reduced graphene layers (GR) were taken into consideration.

Moles of WO_3 = weight of WO_3 / molecular weight of WO_3

The molecular weight of WO_3 is (183.84 g/mol) + 3 * (16.00 g/mol) = 231.84 g/mol.

Weight of WO_3 = 80 mg = 0.080 g (The ratio of WO_3:GR in the composite is 80 mg : 20 mg)

Therefore, moles of WO_3 = 0.080g / 231.84 g/mol = 0.000345066 moles

The accurate number of moles of GR could not be determined without knowing the exact molecular weight of GR which is dependent on numerous factors such as the extent of reduction of graphene oxide (GO), the presence of residual functional groups, and the exact number of layers of graphene. Hence an approximate estimation is deducted from the elemental analysis derived from EDAX measurements in FESEM from Supplementary Figure S4.

Molecular weight from atomic weight percentage of elements in GR

= [(C wt. % /100) * 12.01 g/mol] + [(O wt. % /100) * 16.00 g/mol]

The approximate molecular weight of GR = 12.8115 g/mol

Moles of GR = 0.020g / 12.8115 g/mol = 0.001561097 moles

Total number of moles in the WO_3/GR electrocatalyst is 1.906163 x 10^{-3} moles

At an overpotential of 50 mV, the respective current density, j for the CC@WO_3/GR electrode in the 0.5M H_2SO_4 electrolyte is 7.66 mA cm^{-2} (From Figure 4b).

Therefore TOF = 7.66 x 10^{-3} / (1.906163 x 10^{-3} x 96485.4 x 2) = 0.00208 x 10^{-2} s^{-1}

Similarly, the TOF values were calculated at 75, 100, 125, 150,175, and 200 mV [21] for the electrodes CC@WO_3/GR and SS@WO_3/GR in both the acidic and basic electrolytes and represented in Figure S13 respectively.

References

1. Y. Lv, Y. Liu, C. Chen, T. Wang and M. Zhang, *Electrochim Acta*, 2018, **281**, 1–8.
2. H. Tian, X. Cui, L. Zeng, L. Su, Y. Song and J. Shi, *J Mater Chem A Mater*, 2019, **7**, 6285–6293.
3. T. H. Wondimu, G.-C. Chen, D. M. Kabtamu, H.-Y. Chen, A. W. Bayeh, H.-C. Huang and C. H. Wang, *Int J Hydrogen Energy*, 2018, **43**, 6481–6490.
4. S. Chandrasekaran, P. Zhang, F. Peng, C. Bowen, J. Huo and L. Deng, *J Mater Chem A Mater*, 2019, **7**, 6161–6172.
5. V. Yu. Fominski, S. N. Grigoriev, R. I. Romanov, M. A. Volosova, A. I. Grunin and G. D. Teterina, *Technical Physics Letters*, 2016, **42**, 555–558.
6. S. Y. Toledo Camacho, A. Rey, M. D. Hernández-Alonso, J. Llorca, F. Medina and S. Contreras, *Appl Surf Sci*, 2018, **455**, 570–580.
7. J. Chen, D. Yu, W. Liao, M. Zheng, L. Xiao, H. Zhu, M. Zhang, M. Du and J. Yao, *ACS Appl Mater Interfaces*, 2016, **8**, 18132–18139.
8. R. Rajalakshmi, C. Viswanathan and N. Ponpandian, *Sustain Energy Fuels*, 2021, **5**, 5851–5865.
9. Y. Chen, R. Ren, Z. Wen, S. Ci, J. Chang, S. Mao and J. Chen, *Nano Energy*, 2018, **47**, 66–73.
10. M. Tayebi, Z. Masoumi, M. Kolaei, A. Tayyebi, M. Tayebi, B. Seo, C.-S. Lim, H.-G. Kim and B.-K. Lee, *Chemical Engineering Journal*, 2022, **446**, 136830.
11. Y. Lv, Y. Liu, Y. Liu, Z. Chen and M. Zhang, *J Alloys Compd*, 2018, **768**, 889–895.
12. L. Yang, X. Zhu, S. Xiong, X. Wu, Y. Shan and P. K. Chu, *ACS Appl Mater Interfaces*, 2016, **8**, 13966–13972.
13. X. Zhang, P. Yang and S. P. Jiang, *J Nanostructure Chem*, 2021, **11**, 367–380.
14. R. Choudhary, S. Patra, R. Madhuri and P. K. Sharma, *ACS Sustain Chem Eng*, 2017, **5**, 9735–9748.

15 G. Hu, J. Li, P. Liu, X. Zhu, X. Li, R. N. Ali and B. Xiang, *Appl Surf Sci*, 2019, **463**, 275–282.

16 H. Cheng, M. Klapproth, A. Sagaltchik, S. Li and A. Thomas, *J Mater Chem A Mater*, 2018, **6**, 2249–2256.

17 X. Shang, Y. Rao, S.-S. Lu, B. Dong, L.-M. Zhang, X.-H. Liu, X. Li, Y.-R. Liu, Y.-M. Chai and C.-G. Liu, *Mater Chem Phys*, 2017, **197**, 123–128.

18 X. Xie, W. Mu, X. Li, H. Wei, Y. Jian, Q. Yu, R. Zhang, K. Lv, H. Tang and S. Luo, *Electrochim Acta*, 2014, **134**, 201–208.

19 S. F. Anis and R. Hashaikeh, *Journal of Nanoparticle Research*, 2018, **20**, 47.

20 Anantharaj S, Karthik P, Noda S, *Angewandte Chemie International Edition*, 2021, 60(43), 23051-23067.

21 Roy S, Akbar K, Jeon J, Jerng S, Truong L, Kim K, Yi Y, Chun S, *Journal of Materials Chemistry A*, 2019, 7(36), 20590-20596.